

Numerical simulation of gas transport mechanisms in tight shale gas reservoirs

Yao Jun*, Sun Hai, Fan Dong-yan, Wang Chen-chen and Sun Zhi-xue

School of Petroleum Engineering, China University of Petroleum, Qingdao, Shandong 266580, China

© China University of Petroleum (Beijing) and Springer-Verlag Berlin Heidelberg 2013

Abstract: Due to the nanometer scale pore size and extremely low permeability of a shale matrix, traditional Darcy's law can not exactly describe the combined gas transport mechanisms of viscous flow and Knudsen diffusion. Three transport models modified by the Darcy equation with apparent permeability are used to describe the combined gas transport mechanisms in ultra-tight porous media, the result shows that Knudsen diffusion has a great impact on the gas transport and Darcy's law cannot be used in a shale matrix with a pore diameter less than 1 μm . A single porosity model and a double porosity model with consideration of the combined gas transport mechanisms are developed to evaluate the influence of gas transport mechanisms and fracture parameters respectively on shale gas production. The numerical results show that the gas production predicted by Darcy's law is lower than that predicted with consideration of Knudsen diffusion and the tighter the shale matrix, the greater difference of the gas production estimates. In addition, the numerical simulation results indicate that shale fractures have a great impact on shale gas production. Shale gas cannot be produced economically without fractures.

Key words: Shale gas, gas transport mechanisms, viscous flow, Knudsen diffusion, fracture

1 Introduction

With a rapid decline in conventional petroleum reserves, unconventional resources are playing an increasingly important role in the volatile energy industry over recent years in North America and are gradually becoming a key component in the world's energy supply. Shale gas with huge reserves and extensive distribution represents a significant portion of unconventional natural gas resources and is becoming more important to the global energy supply in years to come (EIA, 2011).

The gas in shale gas reservoirs includes free gas in both fracture and matrix pores and adsorbed gas on the surface of matrix pores (Arogundade and Sohrabi, 2012; Hill and Nelson, 2000; Vermynen, 2011). The main pore size of shale matrix is in the range of 1-200 nm (Javadpour et al, 2007; Loucks et al, 2009; Zou et al, 2012). The widely used Darcy's law cannot be used in shale gas reservoirs because the gas transport in the shale matrix is not conventional viscous flow due to the existence of nanopores (Beskok and Karniadakis, 1999; Civan, 2010; Civan et al, 2011; Javadpour, 2009; Ziarani and Aguilera, 2012). Gas transport in nanopores is a combination of several flow mechanisms including viscous flow, Knudsen diffusion and molecular diffusion, which cannot be described by the Darcy equation (Bird et al, 2002).

Moreover, the adsorption-desorption mechanism also occurs in the pores with adsorbed gas on the surface.

Several transport models have been developed to quantify gas transport in tight porous media with nanometer-size pores (Beskok and Karniadakis, 1999; Civan, 2010; Civan et al, 2011; Ho and Webb, 2006; Javadpour, 2009; Ziarani and Aguilera, 2012). Beskok and Karniadakis (1999) modified the second-order slip approximation to model rarefied gas flow in microchannels, ducts, and pipes. Civan (2010) used the Beskok model (Beskok and Karniadakis, 1999) to describe gas transport in tight porous media. Javadpour (2009) presented a gas transport model in gas shales considering viscous flow and Knudsen diffusion. All these models can describe combined gas transport mechanism in tight porous media; however, no numerical simulations of shale gas reservoirs are presented to investigate the difference in the production predicted by these transport models.

In this paper, a single porosity finite element model was developed and compared with other gas transport models (Darcy equation, the dusty gas model (DGM), Civan model and Javadpour model) for gas production in shale gas reservoirs. Due to the ultra-low permeability, shale gas reservoirs for commercial production are all developed shales with natural fractures (Arogundade and Sohrabi, 2012), which are the main permeable channels with much higher permeability than the matrix. Based on the dual-porosity hypothesis, we treat the shale gas reservoir as a dual porosity system consisting of a matrix system and a fracture system. Gas productions of shale gas reservoirs with different

*Corresponding author. email: RCOGFR_UPC@126.com, yaojunhdpu@126.com

Received June 20, 2013

fracture parameters are compared by numerical simulation to demonstrate the necessity of hydraulic fracturing in shale gas reservoirs.

2 Gas transport mechanisms in tight porous media

2.1 Gas transport mechanisms in shale matrix

Under isothermal condition, gas transport in porous media consists of the following transport mechanisms: viscous flow, Knudsen diffusion and molecular diffusion (Bird et al, 2002; Ho and Webb, 2006). Molecular diffusion refers to the relative motion of different gas species and only occurs in multicomponent gas transport in porous media, while viscous flow and Knudsen diffusion refer to an individual gas species and occur when gas moves in a porous medium. Viscous flow generates from collision between molecules and Knudsen diffusion generates from collision between molecules and the pore walls (as shown in Fig. 1). Among these two mechanisms (viscous flow and Knudsen diffusion), which one is dominant depends on the relationship between the mean free path of gas and the pore size of the porous media. If the mean free path is much smaller than the pore size, the probability of collisions between molecules is much higher than collisions between molecules and the pore walls, thus gas transport is mainly governed by viscous flow resulting from collisions among molecules. As the pore diameters get smaller, reaching the same order as the gas molecular mean free path, collisions between molecules and the pore walls become more important with gas transport mainly governed by Knudsen diffusion than by viscous flow.

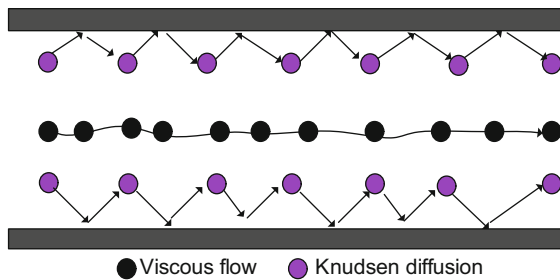


Fig. 1 Schematic of mechanisms of the movement of a single component gas through a porous medium

A widely recognized dimensionless parameter that determines the degree of appropriateness of the continuum model is Knudsen number Kn , which is defined as the ratio of the molecular mean free path λ to the characteristic length scale L , λ is defined as follows (Javadpour et al, 2007):

$$\lambda = \frac{k_B T}{\sqrt{2} \pi \delta^2 p} \tag{1}$$

where k_B is the Boltzmann constant ($k_B=1.3805 \times 10^{-23}$ J/K); T is temperature, K; p is pressure, Pa; and δ is the collision diameter of the gas molecule. The dominant mechanism can be qualified by the Knudsen number. Fig. 2 gives classification of the gas flow regimes and governing equations based on the Knudsen number (Barber and Emerson, 2006; Zhang et al, 2012).

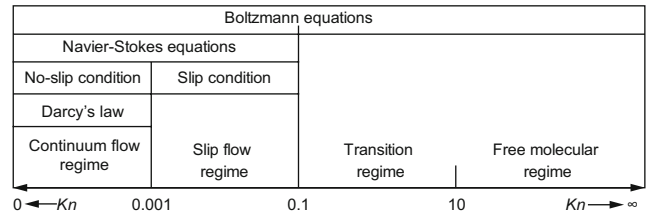


Fig. 2 Classification of the gas flow regimes and governing equations based on the Knudsen number

Gas transport in porous media can be divided into four flow regimes according to the Knudsen number (as shown in Fig. 2):

1) Continuum flow regime, when the Knudsen number is less than 0.001. At this regime, the mean free path of gas is much smaller than the pore size of the porous media, therefore the probability of collisions between molecules is much higher than collisions between the molecules and the pore walls, and the gas transport is mainly governed by viscous flow and Knudsen diffusion can be ignored due to the extremely lower probability of collisions between the molecules and the pore walls. In this regime, both conventional Darcy's law and the Navier-Stokes (N-S) equation with conventional no-slip boundary conditions can describe the gas flow in porous media in the continuum flow regime.

2) Slip flow regime, when $0.001 < Kn < 0.1$. At this regime, the pore size of the porous medium is still larger than the mean free path of gas molecules, the probability of collisions between molecules is still higher than collisions between the molecules and the pore walls, but the probability of collisions between molecules and the pore walls is too high to be ignored. Therefore although viscous flow is still the dominant mechanism, Knudsen diffusion has an effect on the gas transport and cannot be ignored. In this regime, the Darcy equation and no-slip boundary condition fail to describe the gas transport in porous media. However, the N-S equation with slip velocity boundary conditions can be used to describe the gas transport in a porous medium at the slip flow regime.

3) Transition regime, when $0.1 < Kn < 10$. At this regime, the pore size of the porous media is of the same order as the mean free path of gas molecules, the collisions between the molecules and the pore walls become more important and the gas transport is mainly governed by Knudsen diffusion, but viscous flow cannot be ignored. In the transition regime, the continuum assumption and the N-S equations begin to break down, the N-S equations fails to describe gas transport in porous media in the transition regime.

4) Free molecular regime, when $Kn > 10$. At this regime, the pore size is much smaller than the mean free path of gas, the collisions between the molecules and the pore walls are much higher than the inter-molecular collisions, so the gas transport in porous media is governed by Knudsen diffusion and viscous flow can be ignored in the free molecular regime.

The main pore size of the shale matrix is less than $1 \mu\text{m}$, in order to illustrate the gas transport regime in the shale nanopores. Fig. 3 shows the variation of the Knudsen number with pressure at different pore diameters. As shown in Fig.

3, the Knudsen number is almost in the range of 0.001 and 10 within all the pressure from 0.1 to 10 MPa when the pore diameter is less than 1 μm , so the main gas transport regime of shale nanopores is the slip flow regime and the transition regime. Therefore, both the viscous flow and Knudsen diffusion have a great impact on the gas transport in nanopores and the Darcy equation cannot be used to describe gas transport in nanopores.

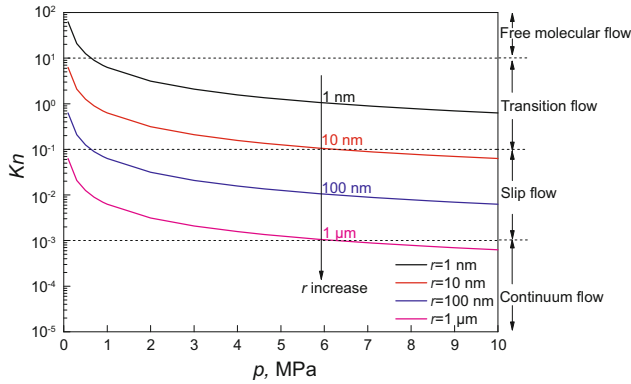


Fig. 3 The Knudsen number and gas flow regime at different pressures and pore diameters

2.2 Gas transport model in shale matrix

Both viscous flow and Knudsen diffusion should be considered in the gas transport in the shale matrix. There are three transport equations available to quantify the combined mechanisms of viscous flow and Knudsen diffusion.

2.2.1 Javadpour model

Javadpour (2009) proposed an apparent permeability equation that considered viscous flow and Knudsen diffusion in a single nanotube.

$$N_t = -\frac{\rho k_a}{\mu} (\nabla p) \quad (2)$$

where N_t is the mass flux of gas transport in the porous media, $\text{kg}/(\text{m}^2 \cdot \text{s})$; μ is the gas viscosity, $\text{Pa} \cdot \text{s}$; ρ is the gas density, kg/m^3 ; k_a is the apparent permeability of the porous media, m^2 , and can be expressed as follows:

$$k_a = \left[\frac{2\mu M}{3RT\rho} \left(\frac{8RT}{\pi M} \right)^{0.5} \frac{8}{r} + \left[1 + \left(\frac{8\pi RT}{M} \right)^{0.5} \frac{\mu}{pr} \left(\frac{2}{\alpha} - 1 \right) \right] \right] k_\infty \quad (3)$$

where M is the molar mass, kg/mol ; R is the universal gas constant; r is the radius of the nanotube, m ; α is the tangential momentum accommodation coefficient (TMAC); k_∞ is the intrinsic permeability of the porous media in m^2 and can be expressed as follows (Choi et al, 2001; Civan et al, 2010):

$$k_\infty = \frac{\phi r^2}{8\tau_h} \quad (4)$$

where ϕ is the porosity of the porous media; τ_h is the tortuosity of the porous media.

2.2.2 Civan model

Civan (2010) used the Beskok and Karniadakis (1999)

model to describe gas transport in tight porous media. The Knudsen number is used to express the apparent permeability.

$$k_a = k_\infty f(Kn) = k_\infty \left(1 + \alpha(Kn)Kn \right) \left(1 + \frac{4Kn}{1 - bKn} \right) \quad (5)$$

where b is the slip coefficient and equal to -1 (for slip flow), $\alpha(Kn)$ is the rarefaction coefficient and given by:

$$\alpha(Kn) = \frac{128}{15\pi^2} \tan^{-1} [4.0Kn^{0.4}] \quad (6)$$

Fig. 4 shows the relationship between k_a/k_∞ and the Knudsen number Kn . As illustrated in Fig. 4, the greater the Knudsen number is, the greater k_a/k_∞ will be, and the greater the impact the Knudsen diffusion will have. According to the Knudsen number the gas transport in porous media can be divided into four regimes:

1) k_a/k_∞ approximately equals 1 when $Kn < 0.001$, which means that viscous flow is the dominant mechanism and Knudsen diffusion can be ignored, Darcy's law can be used when $Kn < 0.001$.

2) k_a/k_∞ is less than 1.48 when Kn is within the range of 0.001 to 0.1, which means viscous flow is still the dominant mechanism but the Knudsen diffusion has an impact on the transport in porous media and cannot be ignored.

3) k_a/k_∞ increases significantly when Kn is within the range of 0.1 to 10, and the Knudsen diffusion is the dominant mechanism rather than viscous flow, but the viscous flow cannot be ignored.

4) k_a/k_∞ is greater than 64 when Kn is greater than 10; this means the Knudsen diffusion is the dominant mechanism and viscous flow can be ignored.

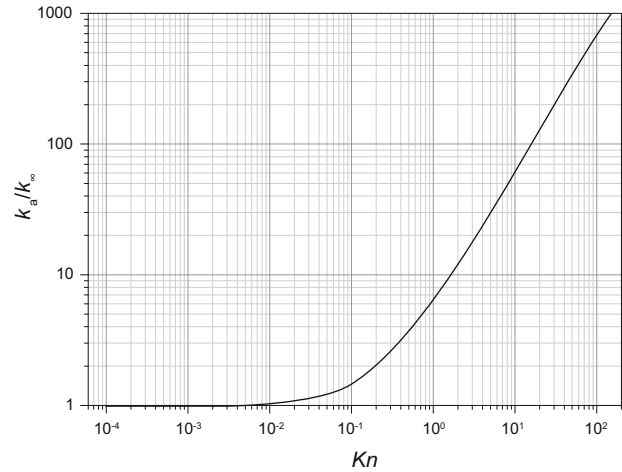


Fig. 4 Variation of k_a/k_∞ with Kn

2.2.3 DGM model

The dusty gas model (DGM) is capable of incorporating mixed mechanisms of viscous flow, Knudsen diffusion and ordinary diffusion (Ho and Webb, 2006), therefore we use the DGM to develop a single component gas transport model in a porous medium:

$$k_a = k_\infty \left(1 + \frac{b_k}{p} \right), \quad b_k = \frac{D_k \mu}{k_\infty} \quad (7)$$

where b_k is the Klinkenberg coefficient, Pa ; D_k is the Knudsen

diffusion coefficient in m^2/s and can be expressed as follows (Florence et al, 2007; Kast and Hohenthanner, 2000):

$$D_k = \frac{\phi}{\tau_h} \frac{2r}{3} \sqrt{\frac{8RT}{\pi M}} \quad (8)$$

2.2.4 Comparison of the apparent permeability equations

The three apparent permeability equations are compared in Fig. 5. A particular case with shale matrix porosity ϕ of 0.05, a single gas component of methane and a temperature of 323.14 K is used for comparison. The computed k_a/k_∞ versus pressure for mean pore diameters of 1 nm, 10 nm, 100 nm, 1 μm and 10 μm are shown in Fig. 5. k_a/k_∞ can be used to quantify the impact of Knudsen diffusion in porous media. When k_a/k_∞ approximates to 1, viscous flow has a greater impact on gas transport than Knudsen diffusion, k_a/k_∞ equaling 1 indicates that the effects of Knudsen diffusion can be neglected; when k_a/k_∞ becomes higher, the impact of Knudsen diffusion increases.

good agreement is shown in the Fig. 5 between the Javadpour model with $\alpha=2$ and the other two models. The apparent permeability calculated by the Javadpour model with $\alpha=0.8$ is much bigger than the other two models.

As shown in Fig. 5, k_a/k_∞ decreases with an increase in pressure, which indicates that the higher pressure is, the smaller k_a/k_∞ is, and the greater effect the viscous flow has. From Fig. 5, it can also be seen that a big pore radius has a small k_a/k_∞ , which indicates that the Knudsen diffusion has a greater impact on gas transport in a porous medium with small pore radii. When the mean pore radius is equal to 1 μm , k_a/k_∞ is close to 1, indicating that Knudsen diffusion is negligible when the mean pore radius is equal to or greater than 1 μm , thus, a single component gas transport in porous media is taken as viscous flow that can be described by Darcy's law. k_a/k_∞ is in the range of 1.4-3.9 when the mean pore radius is equal to 10 nm, and in the range of 1.1-4.7 when the mean pore radius is equal to 100 nm indicating that when the mean pore radius is less than 100 nm, Knudsen diffusion plays an important role in gas transport in porous media.

3 Mathematical model and numerical solution

3.1 Mathematical model

3.1.1 Single porosity model

This model is based on the following assumptions: shale gas reservoirs only consist of a lower-permeable matrix without fractures; gas is stored in the matrix as both a free phase and an adsorbed phase; only a single gas component, CH_4 , is stored in the shale matrix; the gas reservoirs is assumed to be isothermal with gas adsorption on the matrix surface fitting the Langmuir isotherm equation. The classical balance law is written as mass conservation.

Continuity equation for the matrix system in the single porosity model

$$\frac{\partial}{\partial t} (\rho_m \phi_m + (1 - \phi_m) q_{ads}) + \nabla \cdot N_{t,m} = -Q_g \quad (9)$$

where ρ_m is the gas density in the shale matrix, kg/m^3 ; ϕ_m is the porosity of the shale matrix; $N_{t,m}$ is the mass flux of gas transport in the shale matrix in $kg/(m^2 \cdot s)$ and can be expressed as Eq. (2); Q_g is the gas production rate in kg/s and expressed as Eq. (10) (Bustin et al, 2008; Peaceman, 1983); q_{ads} is the amount of gas adsorbed per unit volume in kg/m^3 and can be expressed as Eq.(12) (Civan et al, 2011).

$$Q_g = \frac{\rho_m k_{m,a}}{\mu_m} \frac{\theta}{\ln(r_e / r_w)} (p_m - p_w) \quad (10)$$

where $k_{m,a}$ is the gas apparent permeability in the shale matrix in m^2 and can be expressed as Eqs. (2), (5) and (7); μ_m is the gas viscosity in the matrix system, $Pa \cdot s$; p_m is the matrix pressure, Pa ; if the production well is located at the corner of a grid block, the connect factor θ is $\pi/2$; r_w and p_w are the well bore radius in m and pressure in Pa ; r_e is the equivalent radius in m and can be expressed as follows:

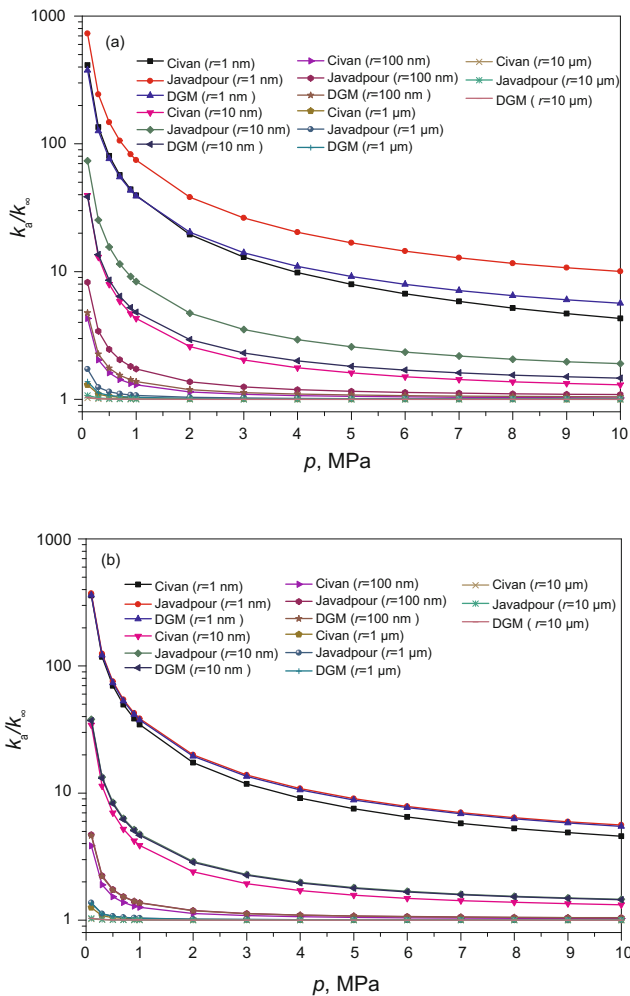


Fig. 5 A comparison of the variation of k_a/k_∞ with pressure computed by different models (a) Considering the slippage effect with $\alpha=0.8$; (b) without considering the slippage effect with $\alpha=2$

It can be seen that the value of the tangential momentum accommodation coefficient, α has a great impact on the apparent permeability calculated by the Javadpour model. A

$$r_e = 0.28 \frac{\left[(k_y / k_x)^{1/2} \Delta x^2 + (k_x / k_y)^{1/2} \Delta y^2 \right]^{0.5}}{(k_y / k_x)^{1/4} + (k_x / k_y)^{1/4}} \quad (11)$$

where k_x and k_y are the permeability in the x and y directions respectively, m^2 ; Δx and Δy are the sizes of well blocks, m.

$$q_{\text{ads}} = \frac{\rho_s M}{V_{\text{std}}} q_{\text{std}} = \frac{\rho_s M}{V_{\text{std}}} \cdot \frac{V_L p}{p_L + p} \quad (12)$$

where ρ_s is the density of the shale matrix, kg/m^3 ; V_{std} is the molar volume at standard conditions (273.15 K and 101.325 kPa), $\text{std m}^3/\text{mol}$; V_L is the Langmuir volume, $\text{std m}^3/\text{kg}$; p_L the Langmuir pressure, Pa; q_{std} is the adsorbed volume per solid mass at standard conditions, $\text{std m}^3/\text{kg}$.

Mathematical model of single porosity

The gas density ρ_m can be written as follows:

$$\rho_m = \frac{p_m M}{ZRT} \quad (13)$$

where Z is the gas deviation factor. By substituting Eqs. (12) and (13) into Eq. (9), we obtain:

$$\left[\gamma \phi_m + \frac{(1 - \phi_m) M_g p_L V_L \rho_s}{V_{\text{std}} (p_L + p_m)^2} \right] \frac{\partial p_m}{\partial t} - \nabla \cdot \left[\gamma \left[\frac{p_m k_{m,a}}{\mu_m} (\nabla p_m) \right] \right] = -Q_g \quad (14)$$

where

$$\gamma = \frac{M}{ZRT} \quad (15)$$

Boundary and initial conditions of the single porosity model

The initial pressure of the shale matrix is p_i in Pa, so the initial condition of the single porosity model is:

$$p_m|_{t=0} = p_i \quad (16)$$

The boundary for solution is $\Gamma = \Gamma_1 + \Gamma_2$, where Γ_1 and Γ_2 represent the outer boundary and the inner boundary of the production well. In this study, we suppose that the outer boundary is sealed and the inner boundary is at constant pressure. The outer boundary condition is:

$$\frac{\partial p_m}{\partial n} \Big|_{\Gamma_1} = 0 \quad (17)$$

where n is the outward unit normal vector of the boundary.

The inner boundary condition is:

$$p_m|_{\Gamma_2} = p_w \quad (18)$$

3.1.2 Double porosity model

This model is based on the following assumptions: shale gas reservoirs consist of a large number of well-connected fractures and a lower-permeable matrix; gas is stored in the natural fractures as a free phase, while in the matrix as both a free phase and an adsorbed phase; only a single component CH_4 is stored in the shale matrix; the gas reservoirs is

assumed to be isothermal with gas adsorption on the matrix surface fitting the Langmuir isotherm equation. We can obtain the continuity equations for the matrix system and the fracture system.

Continuity equation for the matrix system

$$\frac{\partial}{\partial t} (\rho_m \phi_m + (1 - \phi_m) q_{\text{ads}}) + \nabla \cdot N_{t,m} = -Q_p \quad (19)$$

where Q_p is the matrix-fracture mass transfer volume in kg/s and written as follows (Kazemi et al, 1976; Warren and Root, 1963):

$$Q_p = \frac{\rho_m k_{m,a} \alpha^* (p_m - p_f)}{\mu_m} \quad (20)$$

where α^* is the shape factor in $1/\text{m}^2$, $\alpha^* = 4 \left(\frac{1}{L_x^2} + \frac{1}{L_y^2} \right)$; L_x and L_y are the fracture spacing in the x direction and y directions in m respectively.

Continuity equation for the fracture system

$$\frac{\partial}{\partial t} (\rho_f \phi_f) + \nabla \cdot N_{t,f} = Q_p - Q_g \quad (21)$$

where ρ_f is the gas density in fractures, kg/m^3 ; ϕ_f is the fracture porosity; $N_{t,f}$ is the mass flux of gas transport in the shale fracture, $\text{kg}/(\text{m}^2 \cdot \text{s})$; the fracture porosity ϕ_f and intrinsic permeability $k_{f,\infty}$ in m^2 can be calculated by the match-stick model (Bustin et al, 2008).

$$\phi_f = \frac{2b}{a} \quad (22)$$

$$k_{f,\infty} = \frac{b^3}{12a} \quad (23)$$

where a is the average effective fracture spacing, m; b is the fracture aperture width, m.

Mathematical model of double porosity

By substituting Eqs. (12), (13) and (20) into Eqs. (19) and (21), we can obtain the mathematical model of double porosity.

$$\left\{ \begin{array}{l} \left[\gamma \phi_m + \frac{(1 - \phi_m) M_g p_L V_L \rho_s}{V_{\text{std}} (p_L + p_m)^2} \right] \frac{\partial p_m}{\partial t} - \nabla \cdot \left[\gamma \left[\frac{p_m k_{m,a}}{\mu_m} (\nabla p_m) \right] \right] = -\frac{\gamma p_m k_{m,a}}{\mu_m} (p_m - p_f) \\ \left[\gamma \phi_f \right] \frac{\partial p_f}{\partial t} - \nabla \cdot \left[\gamma \left[\frac{p_f k_{f,a}}{\mu_f} (\nabla p_f) \right] \right] = -\frac{\gamma p_m k_{m,a}}{\mu_m} (p_m - p_f) - Q_g \end{array} \right. \quad (24)$$

where the production rate Q_g in the double porosity model is :

$$Q_g = \gamma \frac{p_f k_{f,a}}{\mu_f} \frac{\theta}{\ln(r_e / r_w)} (p_f - p_w) \quad (25)$$

Boundary and initial conditions of the double porosity model

The initial pressure of the shale gas reservoirs is p_i , so the initial condition of the double porosity model is:

$$p_m|_{t=0} = p_f|_{t=0} = P_i \tag{26}$$

The boundary for solution is $\Gamma = \Gamma_1 + \Gamma_2$, where Γ_1 and Γ_2 represent the outer and inner boundaries of the production well. In this study, we suppose the outer boundary is sealed and the inner boundary is at constant pressure. The outer boundary condition is:

$$\frac{\partial p_m}{\partial n}|_{\Gamma_1} = \frac{\partial p_f}{\partial n}|_{\Gamma_1} = 0 \tag{27}$$

The inner boundary condition is:

$$p_f|_{\Gamma_2} = P_w \tag{28}$$

3.2 Numerical solution

The finite element method (FEM) is used to solve the single porosity and double porosity mathematical models of shale gas reservoirs. The finite element method is used to solve the double porosity mathematical model, which is taken as an example to illustrate the solution procedure. The fracture pressure p_f and matrix pressure p_m are solved alternately. The fracture pressure is solved first and then the matrix pressure. The implicit fracture pressure and the explicit matrix pressure are adopted. First the discrete time domain is obtained by forward difference, then by Eq. (24) and Eq. (25) we can obtain the fracture pressure at $n+1$ time steps P_f^{n+1} :

$$\gamma\phi_f \frac{P_f^{n+1} - P_f^n}{t^{n+1} - t^n} - \nabla \cdot \left[\gamma \left[\frac{P_f^n k_{fa}^n}{\mu_f^n} (\nabla P_f^{n+1}) \right] \right] = Q_p^{n+1} - Q_g^{n+1} \tag{29}$$

$$Q_p^{n+1} = \frac{\gamma P_m^n k_{ma}^n}{\mu_m^n} (P_m^n - P_f^n) \tag{30}$$

$$Q_g^{n+1} = \gamma \frac{P_f^n k_{fa}^n}{\mu_f^n} \frac{\theta}{\ln(r_e / r_w)} (P_f^n - P_w) \tag{31}$$

According to the standard Galerkin finite element procedure based on the Galerkin weighted residual method, for a typical finite element, the fracture pressure variable p_f is approximated over an element as follows:

$$p_f \approx \sum_{i=1}^3 N_i P_{f,i} = \mathbf{N}_e \mathbf{P}_{f,e} \tag{32}$$

where $\mathbf{N}_e = [N_1, N_2, N_3]$ is the shape function of pressure, $\mathbf{P}_{f,e} = [p_{f,1}, p_{f,2}, p_{f,3}]$ is the fracture pressure at the element nodal. By using the part integration, the first part of Eq. (29) is transformed and the weak integral form Eq. (33) is obtained, which can satisfy both the governing equation (Eq. (24)) and the Neumann boundary conditions of Eq. (27).

$$\begin{aligned} & \iint_{\Omega_e} \nabla \mathbf{N}_e^T C_f \nabla \mathbf{N}_e d\Omega_e \mathbf{P}_{f,e}^{n+1} - \\ & \gamma\phi_f \iint_{\Omega_e} \mathbf{N}_e^T \mathbf{N}_e d\Omega_e \frac{\mathbf{P}_{f,e}^{n+1} - \mathbf{P}_{f,e}^n}{t^{n+1} - t^n} \\ & = \iint_{\Omega_e} \mathbf{N}_e^T (Q_p^{n+1} - Q_g^{n+1}) d\Omega_e \end{aligned} \tag{33}$$

with

$$C_f = \gamma \frac{P_{f,ae}^n k_{fa}^n}{\mu_f^n}$$

$$P_{f,ae} = \begin{bmatrix} 1 & 1 & 1 \\ 3 & 3 & 3 \end{bmatrix} \mathbf{P}_{f,e}^{nT}$$

$$\nabla \mathbf{N}_e = \begin{bmatrix} \frac{\partial N_1}{\partial x} & \frac{\partial N_2}{\partial x} & \frac{\partial N_3}{\partial x} \\ \frac{\partial N_1}{\partial y} & \frac{\partial N_2}{\partial y} & \frac{\partial N_3}{\partial y} \end{bmatrix}$$

By substituting Eq. (32) into Eq. (33), we obtain Eq. (34).

$$A_f \mathbf{P}_f^{n+1} - R_f \frac{\mathbf{P}_f^{n+1} - \mathbf{P}_f^n}{t^{n+1} - t^n} = \mathbf{Q}_f^{n+1} \tag{34}$$

with

$$A_f = \iint_{\Omega_e} \nabla \mathbf{N}_e^T C_f \nabla \mathbf{N}_e d\Omega_e$$

$$R_f = \gamma\phi_f \iint_{\Omega_e} \mathbf{N}_e^T \mathbf{N}_e d\Omega_e$$

$$Q_f = \iint_{\Omega_e} \mathbf{N}_e^T (Q_p^{n+1} - Q_g^{n+1}) d\Omega_e$$

$$\mathbf{P}_f = [p_{f1}, p_{f2}, \dots, p_{fN_p}]^T$$

where N_p is the number of nodes.

The finite element formulation of gas transport in a double porosity fracture system can be obtained as follows:

$$\left(A_f - \frac{1}{t^{n+1} - t^n} R_f \right) \mathbf{P}_f^{n+1} = \frac{-1}{t^{n+1} - t^n} R_f \mathbf{P}_f^n + \mathbf{Q}_f^{n+1} \tag{35}$$

Then we can obtain the matrix pressure at $n+1$ time steps P_m^{n+1} , similarly we obtain the finite element formulation of double porosity gas transport in a matrix system as follows:

$$\left(A_m - \frac{1}{t^{n+1} - t^n} R_m \right) \mathbf{P}_m^{n+1} = \frac{-1}{t^{n+1} - t^n} R_m \mathbf{P}_m^n + \mathbf{Q}_m^{n+1} \tag{36}$$

with

$$A_m = \iint_{\Omega_e} \nabla \mathbf{N}_e^T C_m \nabla \mathbf{N}_e d\Omega_e$$

$$C_m = \gamma \frac{P_{m,ae}^n k_{ma}^n}{\mu_m^n}$$

$$P_{f,ac} = \left[\frac{1}{3} \frac{1}{3} \frac{1}{3} \right] \mathbf{P}_{f,e}^{nT}$$

$$\mathbf{P}_{m,e} = [p_{m,1}, p_{m,2}, p_{m,3}]$$

$$R_m = \iint_{\Omega_e} \mathbf{N}_e^T D_m \mathbf{N}_e d\Omega_e$$

$$D_m = \gamma \phi_m + \frac{(1 - \phi_m) M_g p_L V_L \rho_s}{V_{std} (\rho_L + P_{mf,ac}^n)^2}$$

$$Q_m = \iint_{\Omega_e} \mathbf{N}_e^T (-Q_{mp}^{n+1}) d\Omega_e$$

$$Q_m^{n+1} = \frac{\gamma P_m^n k_{m,a}^n}{\mu_m^n} (P_m^n - P_f^{n+1})$$

$$\mathbf{P}_m = [p_{m1}, p_{m2}, \dots, p_{mN_p}]^T$$

In this work, the Lagrange interpolation function of element is 2-order for pressure, the Newton-Raphson method is used to solve Eq. (34) and (36) alternately. Similarly we can use the finite element method to solve the single porosity model of shale gas reservoirs.

4 Results and discussion

4.1 Verification of the numerical solution

In order to verify the numerical solution solved by FEM, we compare the numerical solution in this study with the analytical solution of Darcy flow in the double porosity model established by Warren and Root, 1963. Fig. 6 compares the analytical solution with the numerical result obtained by FEM in this paper. Parameters used in this paper are shown in Table 1, there is a gas production well in the center of the reservoir with constant pressure. As shown in Fig. 6, the numerical solution of this paper is consistent with the analytical solution (Warren and Root, 1963), therefore our numerical solution is reliable and feasible.

Table 1 Parameters of the Darcy flow in the double porosity model

Parameter	Value
Initial reservoir pressure, Pa	1×10^7
Well bottom pressure, Pa	1×10^6
Reservoir temperature, K	323
Gas composition	Methane
Matrix permeability, m^2	1×10^{-19}
Matrix porosity	0.05
Fracture permeability, m^2	1×10^{-15}
Fracture porosity	0.001
Wellbore radius, m	0.1

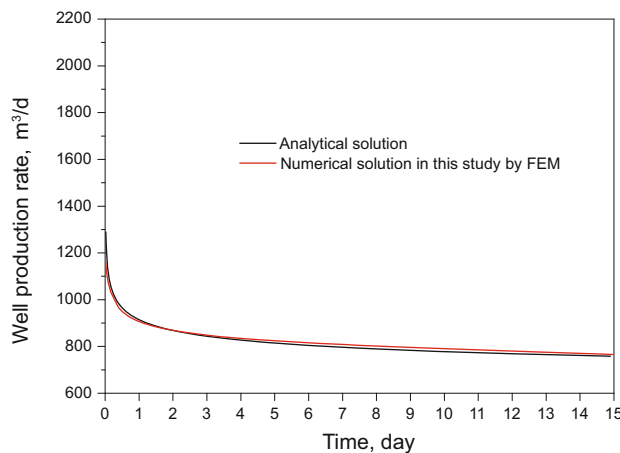


Fig. 6 A comparison of numerical and analytical solutions of the Darcy flow in the double porosity model

4.2 Gas transport behavior in single matrix systems

The single porosity models with different apparent permeabilities calculated by the four transport models (Darcy’s law, Javadpour model, Civan model and DGM model) are modeled to investigate the gas transport behavior in a tight shale matrix.

The performance of a production well with a well spacing of 200 m in a five-spot well pattern (as shown in Fig. 7) is modeled. The basic parameters are shown in Table 2. The intrinsic permeability of the shale matrix is calculated by Eq.(4), the apparent permeability is calculated by the Javadpour, Civan and the DGM models, respectively.

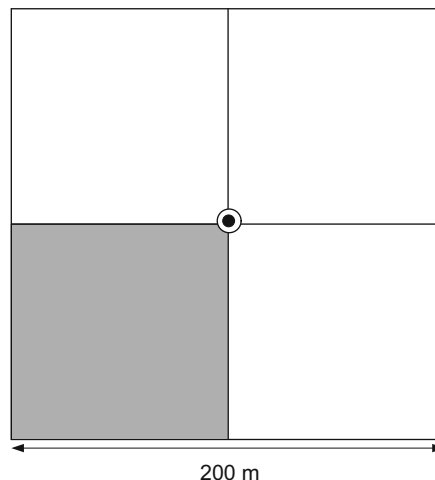


Fig. 7 Well pattern used in the single porosity model

Fig. 8 shows the cumulative production predicted by different transport models (Civan model, DGM, Javadpour model and Darcy model) for the shale matrix with equivalent pore radii of 1, 10 and 100 nm, respectively. As illustrated in Fig. 8, the cumulative production predicted by the transport models considering the combined mechanisms is much higher than that predicted by the Darcy equation. The smaller the mean equivalent pore radius, the greater difference between

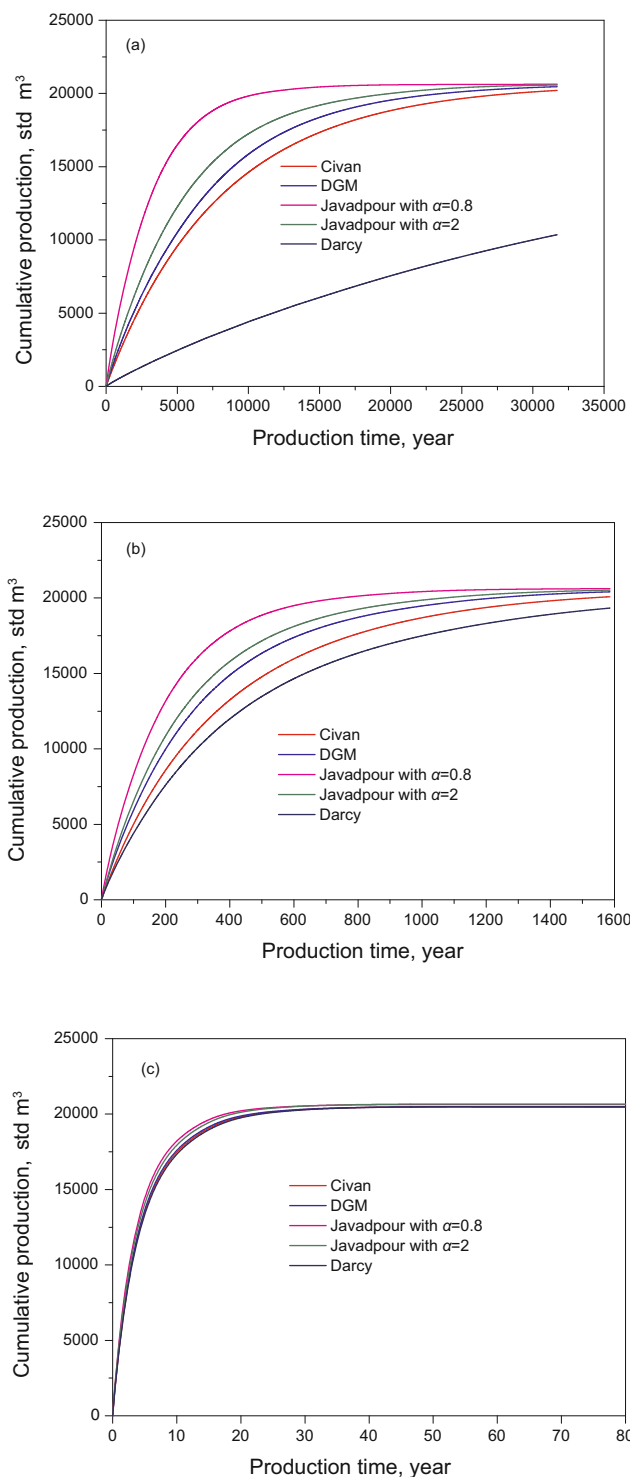


Fig.8 Cumulative production predicted by different transport models in a shale matrix with different mean equivalent pore radii (a) mean equivalent pore radius 1 nm; (b) 10 nm; (c) 100 nm

the predicted cumulative production and the greater the error of the Darcy equation. This indicates that Knudsen diffusion has a great impact on the gas production of shale gas reservoirs with a small equivalent pore radius. The smaller the equivalent pore radius, the greater impact of Knudsen diffusion. When the equivalent pore radius is equal to 100 nm, the production predicted by the Darcy equation is very

close to that predicted by the other models considering the Knudsen diffusion (as shown in Fig. 8(c)).

As shown in Fig. 8, the cumulative production predicted by the Javadpour model considering the slippage effect with $\alpha=0.8$ is greater than that predicted by the other three models (Javadpour model without considering the slippage effect with $\alpha=2$, Civan model and DGM). The predictions of the Javadpour model without considering the slippage effect with $\alpha=2$, the Civan model and the DGM are closer to each other.

Table 2 Basic data used in the single porosity model

Parameter	Value
Initial reservoir pressure, Pa	1.04×10^7
Well bottom pressure, Pa	3.45×10^6
Reservoir temperature, K	323
Gas composition	100% methane
Mean equivalent pore radius, nm	1, 10, 100
Matrix porosity	0.05
Wellbore radius, m	0.1
Fracture	No fracture
Shale density, kg/m^3	2600
Langmuir volume, m^3/kg	2.8317×10^{-3}
Langmuir pressure, Pa	1.04×10^7

4.3 Effects of fracture parameters on the gas production

The double porosity model was used to investigate the performance of gas production of shale gas reservoirs with fractures. The performance of a production well with a well spacing of 400 m in a five-spot well pattern (similarly to that shown in Fig. 7 but with a different well spacing of 400 m) was modeled. The mean equivalent pore radius of the shale matrix is 10 nm, the fracture aperture width is 5 μm , the fracture spacing are 0.05, 0.10, 0.20, 0.50, 1 and 5 m, respectively, the intrinsic permeability and porosity are calculated by Eqs. (22) and 23, other parameters are shown as in Table 2.

The influence of the fracture spacing on the cumulative production and production rate are shown in Fig. 9. As illustrated in Fig. 9, shale fractures have a great impact on the gas production of shale gas reservoirs. The production rate of a shale gas reservoir with a fracture spacing of 0.05 m is more than 500 times of that of a shale gas reservoir without fractures. A shale gas reservoir without fractures has no commercial production rate.

Fig. 10 shows the variation of the average ratio of apparent permeability and intrinsic permeability in the shale matrix and fracture systems, respectively. As illustrated in Fig. 10, the ratio of apparent permeability to intrinsic permeability in the shale fracture is approximately equal to 1 in all the production time, which means that the Knudsen diffusion has little impact on the gas transport in the shale fracture and can be ignored. However, the ratio of apparent

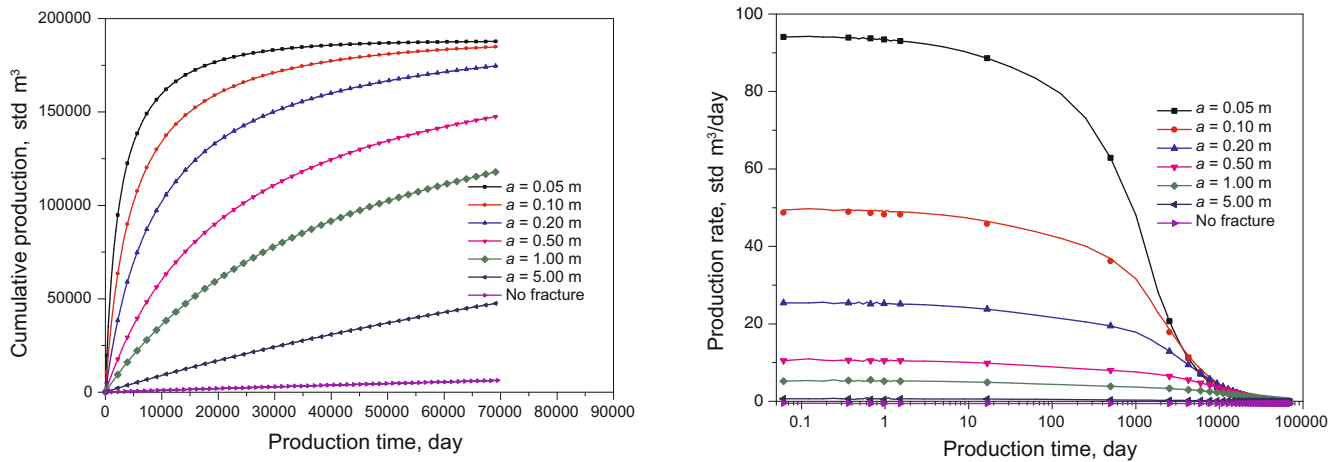


Fig. 9 Effects of fracture spacing on cumulative production and production rate

permeability to intrinsic permeability in the matrix increases with production time, from the initial permeability ratio 1.7 to 6.15 at the last production time, which indicates that the Knudsen diffusion has a great impact on the gas transport in the shale matrix.

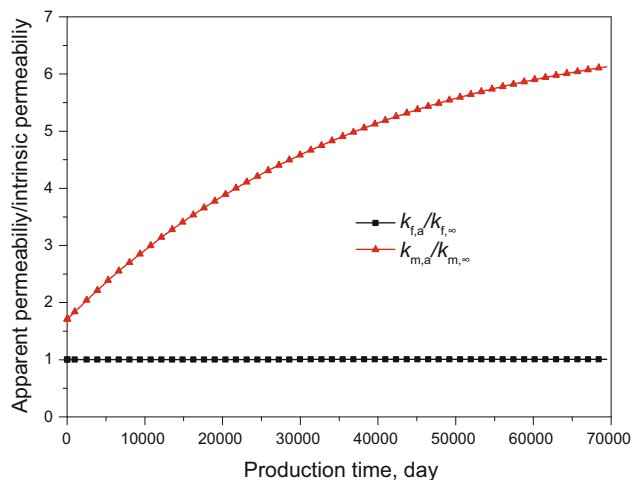


Fig. 10 Variation of the average ratio of apparent permeability to intrinsic permeability of the matrix and fracture systems in shale gas reservoirs

5 Conclusions

In this study, we investigated gas transport mechanisms in tight porous media and compare the gas transport models (Javadpour, Civan and DGM models) considering the combined mechanisms of Knudsen diffusion and viscous flow. A single porosity finite element model and a double porosity finite element model were developed to investigate the gas production performance in shale gas reservoirs.

1) According to the Knudsen number, gas transport in a porous medium can be divided into four flow regimes: a) continuum flow regime with a Knudsen number, Kn , less than 0.001; b) slip flow regime with $0.001 < Kn < 0.1$; c) transition regime with $0.1 < Kn < 10$; d) free molecular regime

with $Kn > 10$. Viscous flow is the dominant mechanism in regimes a and b while Knudsen diffusion is the dominant mechanism in regimes c and d, neither the Knudsen diffusion nor viscous flow can be ignored in regimes b and c due to their great impact on the gas transport in regimes b and c, however Knudsen diffusion and viscous flow can be ignored in regimes a and d, respectively.

2) Three transport equations (Civan model, Javadpour model and DGM) can describe the combined mechanism of viscous flow and Knudsen diffusion. Knudsen diffusion has a great impact on the gas transport in a porous medium with a small pore radius but Knudsen diffusion can be ignored when the mean pore radius is equal to or greater than $1 \mu\text{m}$. The numerical simulation results show that the production rate predicted by the Darcy equation is lower than that predicted by the transport models considering the combined mechanisms, and the smaller the mean equivalent pore radius, the greater difference between the predicted production rates. The production predicted by the three transport equation (Civan model, Javadpour model and DGM) are not identical, we should further investigate transport equations considering combined transport mechanisms in tight porous media.

3) Fractures are the main permeable channels in the shale gas reservoirs. Shale fractures have a great impact on the gas production of shale gas reservoirs, and those without fractures have no commercial production rate.

Acknowledgements

This work was supported by the National Natural Science Foundation of China (No. 51234007, No. 11072268), Program for Changjiang Scholars and Innovative Research Team in University (IRT1294), the Major Programs of Ministry of Education of China (No. 311009), Specialized Research Fund for the Doctoral Program of Higher Education (No. 20110133120012), the National Natural Science Foundation of Shandong Province (No. 11072268), the Fundamental Research Funds for the Central Universities (No. 11CX05007A), the Fundamental Research Funds for the Central Universities (No. 11CX04022A), and Introducing Talents of Discipline to Universities (B08028).

References

- Arogundade O and Sohrabi M. A review of recent developments and challenges in shale gas recovery. SPE Saudi Arabia Section Technical Symposium and Exhibition, 8-11 April 2012, Al-Khobar, Saudi Arabia (paper SPE 160869)
- Barber R W and Emerson D R. Challenges in modeling gas-phase flow in microchannels: from slip to transition. *Heat Transfer Engineering*. 2006. 27(4): 3-12
- Beskok A and Karniadakis G E. Report: a model for flows in channels, pipes, and ducts at micro and nano scales. *Microscale Thermophysical Engineering*. 1999. 3(1): 43-77
- Bird R B, Stewart W E and Lightfoot E N. *Transport Phenomena* (2nd Edition). New York, USA: John Wiley & Sons, Inc. 2002
- Bustin A M M, Bustin R M and Cui X. Importance of fabric on the production of gas shales. SPE Unconventional Reservoirs Conference, 10-12 February 2008, Keystone, Colorado, USA (paper SPE 114167)
- Choi J G, Do D D and Do H D. Surface diffusion of adsorbed molecules in porous media: monolayer, multilayer, and capillary condensation regimes. *Industrial & Engineering Chemistry Research*. 2001. 40(19): 4005-4031
- Civan F. Effective correlation of apparent gas permeability in tight porous media. *Transport in Porous Media*. 2010. 82(2): 375-384
- Civan F, Rai C S and Sondergeld C H. Intrinsic shale permeability determined by pressure-pulse measurements using a multiple-mechanism apparent-gas-permeability non-Darcy model. SPE Annual Technical Conference and Exhibition, 19-22 September 2010, Florence, Italy (paper SPE 135087)
- Civan F, Rai C S and Sondergeld C H. Shale-gas permeability and diffusivity inferred by improved formulation of relevant retention and transport mechanisms. *Transport in Porous Media*. 2011. 86(3): 925-944
- EIA. *World Shale Gas Resources: An Initial Assessment of 14 Regions Outside the United States*. Washington: U.S. Energy Information Administration. 2011
- Florence F A, Rushing J, Newsham K E, et al. Improved permeability prediction relations for low permeability sands. Rocky Mountain Oil & Gas Technology Symposium, 16-18 April 2007, Denver, Colorado, U.S.A. (paper SPE 107954)
- Hill D G and Nelson C R. Gas productive fractured shales: an overview and update. *Gas TIPS*. 2000. 6(2): 4-13
- Ho C K and Webb S W. *Gas Transport in Porous Media*. Netherlands: Springer. 2006
- Javadpour F. Nanopores and apparent permeability of gas flow in mudrocks (shales and siltstone). *Journal of Canadian Petroleum Technology*. 2009. 48(8): 16-21
- Javadpour F, Fisher D and Unsworth M. Nanoscale gas flow in shale gas sediments. *Journal of Canadian Petroleum Technology*. 2007. 46(10): 55-61
- Kast W and Hohenthanner C R. Mass transfer within the gas-phase of porous media. *International Journal of Heat and Mass Transfer*. 2000. 43(5): 807-823
- Kazemi H, Merrill JR. L S, Porterfield K L, et al. Numerical simulation of water-oil flow in naturally fractured reservoirs. *SPE Journal*. 1976. 16(6): 317-326
- Loucks R G, Reed R M, Ruppel S C, et al. Morphology, genesis, and distribution of nanometer-scale pores in siliceous mudstones of the Mississippian Barnett Shale. *Journal of Sedimentary Research*. 2009. 79(12): 848-861
- Peaceman D W. Interpretation of well-block pressures in numerical reservoir simulation with nonsquare grid blocks and anisotropic permeability. *SPE Journal*. 1983. 23(3): 531-543
- Vermilyen J P. *Geomechanical Studies of the Barnett Shale, Texas, USA*. Palo Alto, California, USA: Stanford University. 2011
- Warren J E and Root P J. The behavior of naturally fractured reservoirs. *SPE Journal*. 1963. 3(3): 245-255
- Zhang W M, Meng G and Wei X. A review on slip models for gas microflows. *Microfluidics and Nanofluidics*. 2012. 13(6): 845-882
- Ziarani A S and Aguilera R. Knudsen's permeability correction for tight porous media. *Transport in Porous Media*. 2012. 91(1): 239-260
- Zou C, Zhu R, Wu S, et al. Types, characteristics, genesis and prospects of conventional and unconventional hydrocarbon accumulations: taking tight oil and tight gas in China as an example. *Acta Petrolei Sinica*. 2012. 33: 173-187 (in Chinese)

(Edited by Sun Yanhua)